

Triggered Superradiance and Spin Inversion Storage in a Hybrid Quantum System

Wenzel Kersten,^{1,*} Nikolaus de Zordo,¹ Oliver Diekmann,² Tobias Reiter,² Matthias Zens,² Andrew N. Kanagin,¹ Stefan Rotter,² Jörg Schmiedmayer,¹ and Andreas Angerer¹

¹ Vienna Center for Quantum Science and Technology, Atominstitut, TU Wien, Stadionallee 2, A-1020 Vienna, Austria

² Institute for Theoretical Physics, TU Wien, Wiedner Hauptstraße 8-10/136, A-1040 Vienna, Austria

(Dated: January 11, 2023)

We study the superradiant emission of an inverted spin ensemble strongly coupled to a superconducting cavity. After fast inversion, we detune the spins from the cavity and store the inversion for tens of milliseconds, during which the remaining transverse spin components disappear. Switching back on resonance enables to study the onset of superradiance. A weak trigger pulse of a few hundred photons shifts the superradiant burst to earlier times and imprints its phase onto the emitted radiation. For long hold times, the inversion decreases below the threshold for spontaneous superradiance. There the energy stored in the ensemble can be used to amplify microwave pulses passing through the cavity.

Superradiance is the process by which an ensemble of excited two-level systems synchronizes to produce a short, highly coherent burst of light [1]. The build-up of correlations during the collective decay, mediated by an enhanced coupling to a common mode, gives rise to non-linear scaling of the decay rate with the number of emitters [2]. Superradiant (SR) emission is not only fundamental to many fields of physics, but also attracts increasing interest for applications in metrology [3], laser physics [4–6] and quantum technology in general [7–12]. SR phenomena are at the heart of the transition from a genuine quantum regime, where individual fluctuations of the vacuum field will jump-start the collective decay of inverted emitters, to the classical regime, where the emission is akin to that of a macroscopic radiating dipole.

While experiments on superradiance have recently been successfully transferred from atomic ensembles to solid-state spin systems [13, 14], the possibilities this opens up for controlling and exploiting superradiance for applications have been very little explored so far. Progress in this direction has primarily been hindered by the fact that systems giving rise to superradiance are fundamentally unstable, reacting to the slightest disturbance. Although this extreme sensitivity even to weak signals poses a great challenge for experimental implementation, it also offers very promising possibilities for applications in sensor and detector technology [3, 15].

In this work we report on a novel experimental platform that allows us not only to invert a large ensemble of nitrogen-vacancy (NV) spins, but also to hold and stabilize the stored inversion for up to 20 ms – four orders of magnitude longer than the timescale of the SR decay process. This stabilization lets us study and control the emission of a SR burst that releases the energy stored in the ensemble. To trigger the SR emission, we use weak microwave (MW) pulses. Additionally, we investigate a regime with reduced inversion, where the spins act as a gain medium for the amplification of a series of short MW pulses.

In order to coherently manipulate spins with high fi-

delity, we use a newly developed MW resonator [see Fig. 1(a)]. Our setup is based on two opposing superconducting chips that exhibit a small mode volume with homogeneous coupling strength, while retaining a high quality factor of $Q = 3000$ (unloaded $Q = 30000$). This design allows us to reach the regime of strong collective spin-cavity coupling already with a number of NVs that is reduced by three orders of magnitude compared to earlier works [16, 17]. Moreover, owing to the resonator’s compact design, we are able to add a small loop of superconducting wire in order to magnetically tune the spins in and out of the cavity resonance faster than the SR timescale.

The resonator is composed of two sapphire chips with a 200 nm thin layer of $16 \times 16 \text{ mm}^2$ superconducting Niobium mounted in a copper housing. The identical patterns on both chips feature a hole in the center from which a $4 \mu\text{m}$ slit reaches outwards, resembling a split ring resonator [18]. The chips are stacked, with the roughly cube shaped diamond sample placed between the center holes. The hole radii, the distance between the chips and the sample size are all of similar dimension $d \sim 200 \mu\text{m}$. This configuration results in a resonance frequency of $\omega_c/2\pi = 3.1 \text{ GHz}$ and linewidth of $\kappa/2\pi = 0.5 \text{ MHz}$ (HWHM). The resonator’s oscillating magnetic field couples homogeneously to all spins with a collective coupling strength of $g_{\text{coll}}/2\pi = 5.2 \text{ MHz}$. The NV sample has a number of 3.6×10^{13} spins with an effective linewidth for the inhomogeneously broadened spin ensemble of $\Gamma_{\perp}/2\pi = 4.3 \text{ MHz}$ [19], a value that takes the spin frequency distribution, modeled by a q -Gaussian function [20], into account (see Supplemental Material). The resulting cooperativity parameter of our coupled system is $C = g_{\text{coll}}^2/(\kappa\Gamma_{\perp}) \approx 12.2$.

We begin our explorations with all NV spins as effective two-level systems thermally relaxed to the ground state. The spins are then inverted using a 400 ns modified chirp pulse with a Gaussian envelope. Details of the initialization procedure are given in the Supplemental Material. Following the inversion pulse, we rapidly switch off the

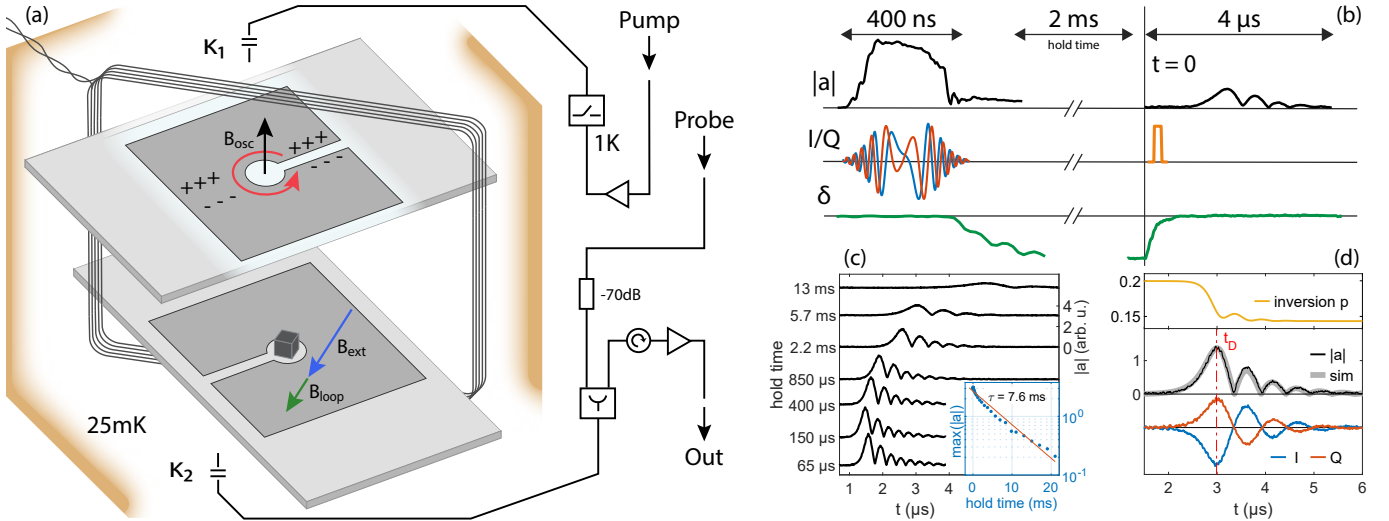


FIG. 1. (a) Schematic of the MW cavity located in a dilution refrigerator operating at 25 mK and connected to a homodyne MW setup. Two sapphire chips with opposing split ring structures and the diamond sample are stacked inside a copper box. Between the center holes the oscillating magnetic field homogeneously penetrates the sample. The chips are surrounded by a loop made of 5 windings of superconducting wire, enabling a rapid detuning of the spins. The pin coupler of port 1 is connected to the pump-line, which can be decoupled from the room temperature thermal bath at the 1 K stage using a solenoid switch. Port 2 is connected to the out-line for acquiring data, and the attenuated probe-line for injecting weak trigger pulses. (b) Sequence of the experiment. We use a modified chirp pulse (red/blue) to invert the spin ensemble and subsequently detune the spins by switching off the current (green) in the loop, thereby storing the inversion. After a certain hold time we bring the spins back into resonance and see their SR decay (black), optionally triggered by a short probe pulse (orange). (c) SR decays for varying hold times, triggered by room temperature noise. The inset shows the SR decay maxima together with an exponential fit in a semi-log plot. (d) Example data and simulation of a SR decay and its associated quadrature values I/Q , together with the simulated inversion p . The vertical line indicates t_D , the time of the maximum cavity amplitude.

loop current in about 200 ns using a semiconductor switch, causing a detuning of the spins by $\delta/2\pi = 26$ MHz. This detuning by more than the ensemble linewidth inhibits the SR interaction of the spin ensemble with the cavity mode, thereby storing the inversion [19].

During the inversion hold time, dephasing processes eliminate the spins' collective dipole moment determined by the transversal component of the collective spin vector, $S_- = S_x - iS_y$. When tuning the ensemble back into resonance, we thus create a metastable inverted state whose tipping angle $\theta = \arctan(|S_-|/S_z)$ with respect to the z -axis in the Bloch sphere is exponentially decreased for longer hold times. Under the condition that the product of the stored ensemble inversion $-1 \leq p \leq +1$ and cooperativity is above the threshold $pC > 1$, this metastable state will decay by emitting a SR photon burst [19]. Here, the inversion parameter p is implicitly defined by $S_z = \frac{1}{2}\langle \sum_j \sigma_z^j \rangle = pN/2$. In this state, the presence of even a single photon in the cavity will stimulate the collective emission of radiation, starting a self-accelerating photonic avalanche. During this process, the energy released in the form of cavity photons gradually builds up, reaches a maximum and then oscillates back and forth between the two subsystems, before the process stops due to the dephasing of the spins and their decoherence. The full experimental sequence is summarized in Fig. 1(b).

Our first notable result is presented in Fig. 1(c), where we plot the SR decay pulses for varying inversion hold times. Here, the SR decay is triggered by noise from the high power amplifier of the pump-line. The measured SR dynamics are captured in a semi-classical description using the Maxwell-Bloch equations [21]. We model the time evolution starting from an inverted state with a slight tipping angle accounting for fluctuations that initiate the SR decay (see Supplemental Material). To simulate the measured signals of $|a|$ we only adjust the ensemble inversion p and a time offset, resulting in curves as shown in Fig. 1(d). The role of fluctuations at the start of the SR decay process is studied in more detail below. We find the decay maximum $\max(|a|)$, an indirect measure of the energy stored by the spins, to decrease roughly exponentially with increasing hold times, exhibiting a characteristic timescale of $\tau = 7.6$ ms [see inset Fig. 1(c)]. For hold times longer than 20 ms, the inversion has already decreased below the threshold $pC = 1$ for spontaneous superradiance. We hypothesize two distinct timescales for the relaxation of the inverted state; a fast one that rapidly thermalizes the ensemble, driven by spin-spin interactions involving NVs with very short lifetimes (so called *fluctuators* [22]), and a slow one which brings them to the ground state over extended times ($T_1 = 134$ s, see Supplemental Material [23]).

We now focus on the onset of the SR decay process and the possibility to trigger it prior to its self-decay. Using a 2 ms hold time, we give the cavity mode enough time to reach thermal equilibrium after the inversion pulse and subsequent decoupling from the high power amplifier noise by the solenoid switch, with an estimated number of $\bar{n} \approx 2$ thermal photons remaining. The completely dephased inverted state, that is brought back into resonance, has zero tipping angle apart from unavoidable quantum and thermal fluctuations. Another 150 ns after switching back the detuning current (defined as $t = 0$), we send a 100 ns trigger pulse through the highly attenuated MW probe line. The pulse is resonant with the cavity and contains a calibrated number of photons (see Supplemental Material [24]). The experiment is repeated many times for varying numbers of trigger photons, and without trigger pulse. For every run, we extract the delay time t_D and the I_D/Q_D quadrature values of the SR decay maximum [cf. Fig. 1(d)]. We post-select the runs for $\max(|a|) = \sqrt{I_D^2 + Q_D^2}$ to fall into a narrow window, as there is some variation in the initial spin inversion between the runs. The SR decay phases $\varphi = \arctan(Q_D/I_D)$ are corrected for a linear phase drift with t_D , caused by a minor constant detuning of the spins (see Supplemental Material). The resulting sets of delay times and phases is summarized in Figs. 2(a) and 2(b). Clearly, stronger trigger pulses with higher numbers of photons n_{trig} lead to earlier t_D values and narrower distributions for t_D and φ . While our simulation allows to describe the decay process starting from a slightly tipped initial collective spin vector, it is the randomness in the initial conditions that leads to the observed variance in time and phase. These thermal and quantum fluctuations are not included in our semi-classical model. To understand these phenomena and model the distributions of times and phases of the decay pulses, we split the analysis of the SR decay into two stages [2, 15, 25].

The decay process starts with a linear stage, in which the (optional) trigger pulse leads to a coherent rotation of the collective spin vector about an axis defined by the phase of the pulse, which is kept identical for all runs. Prior to this rotation, the initial state is located very close to the $+z$ -axis but with a small tipping angle $\theta = \arctan(|S_-|/S_z)$ and random polar angle $\phi = \arg(S_-)$. As $\cos \theta \simeq 1$ throughout the linear phase, we can treat the spin vector to be confined to a plane with a z -offset corresponding to the initial inversion. The geometric construction of this plane is illustrated in Fig. 2(c), mathematical formulas of the distribution functions are given in the Supplemental Material citerice1945mathematical,angularmarginalization. The initial state of the spin vector follows a two dimensional Gaussian distribution of width $\bar{\theta}$ centered at $\theta = 0$. The influence of the trigger pulse then causes a displacement in the plane, which we choose to be in the direction of $\phi = 0$. The parameter η expresses the displacement in units of

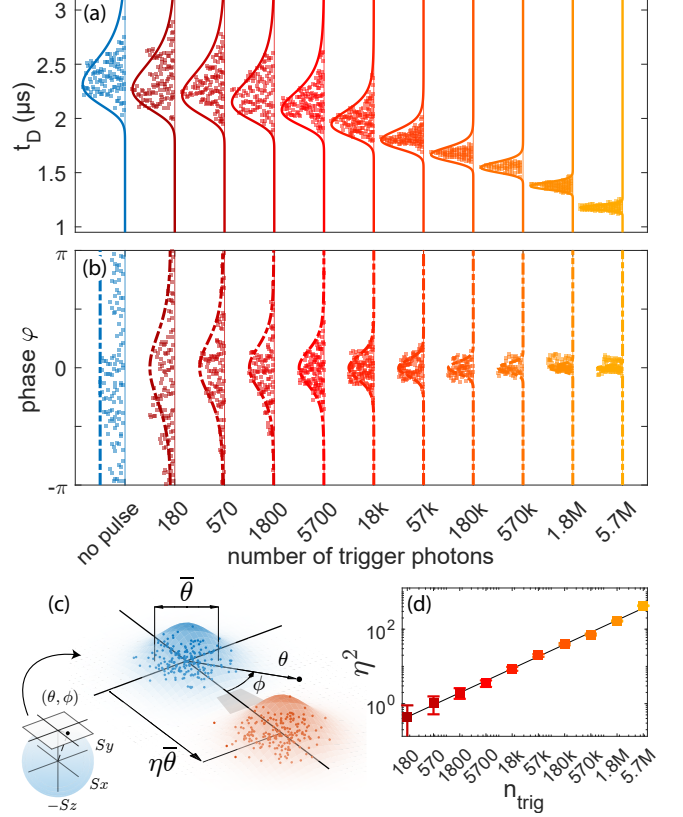


FIG. 2. Swarm plots of the measured delay times t_D (a) and phases φ (b) of the SR decay maxima in over 1200 runs with varying powers (photon numbers) of the 100 ns trigger pulse, or no pulse at all. The distributions plotted using solid lines in (a) correspond to the maximum likelihood estimates for the displacement parameter η to the recorded t_D data, where other parameters are kept fixed. The dashed lines in (b) are the expected phase distributions for those estimates of η . (c) Initial state of the collective spin vector with coordinates (θ, ϕ) close to the north pole of the Bloch sphere. In-plane distribution before (blue) and after (red) the coherent displacement η in units of the width $\bar{\theta}$ via the trigger pulse. (d) Log-log plot of the squared displacement η^2 over the estimated number of trigger photons in the cavity.

the width parameter $\bar{\theta}$. For growing η , i.e., higher trigger pulse powers, the initially randomly distributed polar angles become increasingly well defined and approach a narrow distribution around $\phi = 0$ [see Fig. 2(b)].

After this linear stage, where the collective spin vector is coherently displaced from its random in-plane starting position, we enter a nonlinear regime. Now the SR dynamics dominate and via a collective process of stimulated emission the spin vector accelerates its rotation towards the equator while emitting a considerable burst of MW radiation.

The phase φ of the emitted decay pulse is directly determined by the value of ϕ at the start of the nonlinear stage. Less directly, we can infer the initial tipping angles θ from the delay times t_D , which result via the relation

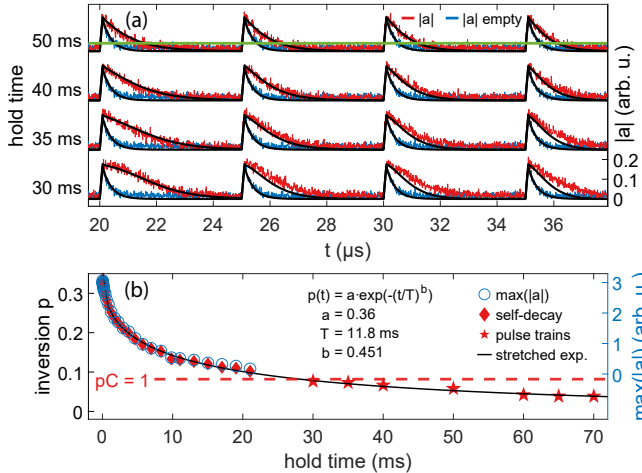


FIG. 3. (a) Cavity amplitude $|a|$ for a series of 100 ns pulses, each injecting $n_{\text{trig}} \approx 4.1 \times 10^9$ photons, amplified by the partially inverted spin ensemble in the reduced effective cooperativity regime $pC < 1$ for different hold times (red). In comparison, we plot the signal obtained with an empty cavity where spins are far detuned (blue). For choosing the parameters in our semi-classical model (black), we ignore noise below a certain threshold (green line at the top). (b) Ensemble inversion p as a function of hold time, extracted by simulations in the two regimes above and below $pC = 1$. Above this threshold, the pulse maxima (right y -axis) follow the values of p from simulations of the self-decays shown in Fig. 1(c). A stretched exponential is fitted to the inversion as a guide to the eye.

$t_D = -2T_R \log(\theta/2)$ [15]. Here, the parameter T_R represents the timescale for the SR emission process (see Supplemental Material). With this relation and the assumed distribution for the initial tipping angles θ depending on η [see Fig. 2(c)], we can reproduce the distributions of the measured t_D data using maximum likelihood estimation to fit η . For that, we fix the values $T_R = 212$ ns and $\bar{\theta} = 6 \times 10^{-3}$ using the measurement runs without probe pulses ($\eta = 0$). In Fig. 2(a) we show the resulting t_D distributions from these estimates of η . The corresponding phase distributions in Fig. 2(b) are not fitted, but result directly from those η estimates.

As the displacement η is caused by the MW magnetic field of the trigger pulse, its square is a measure of the energy imparted onto the spin system during the linear stage of the SR process. Therefore, the number of photons that trigger the SR decay is proportional to $\eta^2 \propto n_{\text{trig}}$ [see Fig. 2(d)]. Remarkably, a weak MW pulse on the order of 10^{-11} photons per spin is sufficient to have an observable effect on the SR decay. This observation opens the perspective to operate our system as a detection device that is not only sensitive to the amplitude, but also the phase of weak MW signals.

We now investigate a regime of reduced effective cooperativity $pC < 1$, where SR emission does not occur spontaneously [19]. To that end, we employ hold times longer than 20 ms, thus reducing the polarization below

the threshold for the SR decay. We probe the system by injecting, at 5 μ s intervals, a sequence of resonant MW pulses of 100 ns duration via the pump-line. Interestingly, in Fig. 3(a), we find that this results in an amplification of the pulses as compared to the empty cavity response (with far detuned spins). Although no spontaneous SR decay occurs on its own, it is still possible to repeatedly extract energy from the stored inversion. The incident pulses hereby effectively supply the necessary coherence that is otherwise constituent to the SR emission, but hindered from building up when the stored inversion is insufficient. Notably, tens of injected MW pulses can be amplified in succession. We are able to replicate the measured dynamics using our numerical model with only the amplitude of the incident pulses (kept fixed for all fits) and the ensemble inversion p as free parameters. These results are combined in Fig. 3(b) with the p values attained by simulating the SR self-decays [cf. Fig. 1(d)]. The semi-classical model seamlessly captures the behavior of our system in both regimes of high and low effective cooperativity.

In summary, we present and successfully operate an experimental platform to store the energy of an inverted spin ensemble for tens of milliseconds and to release it via a strong SR burst. By initializing the system to a fully upright inverted state, we demonstrate a high sensitivity to weak MW pulses that strongly influence the subsequent SR dynamics, allowing us to infer both amplitude and phase of the trigger pulse. The decrease of inversion over time allows us to study a regime of reduced cooperativity without spontaneous SR emission, where the inverted spins effectively act as a gain medium for a series of short MW pulses. Our setup lays the ground work for the design of highly sensitive MW detectors on a chip.

We thank Johannes Majer for discussions and technical support in the initial phases of the project. We acknowledge support by the Austrian Science Fund (FWF) projects I3765 (MICROSENS), P34314 (Spins in Quantum Solids) and P32300, and by the European Union’s Horizon 2020 research and innovation programme (FET-OPEN project FATMOLS, Grant No. 862893) as well as by the Studienstiftung des Deutschen Volkes.

* wenzel.kersten@tuwien.ac.at

- [1] R. H. Dicke, Physical review **93**, 99 (1954).
- [2] M. Gross and S. Haroche, Physics reports **93**, 301 (1982).
- [3] M. Koppenhöfer, P. Groszkowski, H.-K. Lau, and A. A. Clerk, PRX Quantum **3**, 030330 (2022).
- [4] J. G. Bohnet, Z. Chen, J. M. Weiner, D. Meiser, M. J. Holland, and J. K. Thompson, Nature **484**, 78 (2012).
- [5] Y. Zhang, C. Shan, and K. Mølmer, Physical Review Letters **126**, 123602 (2021).

- [6] Q. Wu, Y. Zhang, X. Yang, S.-L. Su, C. Shan, and K. Mølmer, *Science China Physics, Mechanics & Astronomy* **65**, 1 (2022).
- [7] A. Kuzmich, W. Bowen, A. Boozer, A. Boca, C. Chou, L.-M. Duan, and H. Kimble, *Nature* **423**, 731 (2003).
- [8] D. Yang, S.-h. Oh, J. Han, G. Son, J. Kim, J. Kim, M. Lee, and K. An, *Nature Photonics* **15**, 272 (2021).
- [9] J. Kim, D. Yang, S.-h. Oh, and K. An, *Science* **359**, 662 (2018).
- [10] R. Pennetta, D. Lechner, M. Blaha, A. Rauschenbeutel, P. Schneeweiss, and J. Volz, *Physical Review Letters* **128**, 203601 (2022).
- [11] M. O. Araújo, I. Krešić, R. Kaiser, and W. Guerin, *Physical review letters* **117**, 073002 (2016).
- [12] J. Kim, S.-h. Oh, D. Yang, J. Kim, M. Lee, and K. An, *Nature Photonics* **16**, 707 (2022).
- [13] A. Angerer, K. Streltsov, T. Astner, S. Putz, H. Sumiya, S. Onoda, J. Isoya, W. J. Munro, K. Nemoto, J. Schmiedmayer, *et al.*, *Nature Physics* **14**, 1168 (2018).
- [14] J. Q. Quach, K. E. McGhee, L. Ganzer, D. M. Rouse, B. W. Lovett, E. M. Gauger, J. Keeling, G. Cerullo, D. G. Lidzey, and T. Virgili, *Science advances* **8**, eabk3160 (2022).
- [15] P. Goy, L. Moi, M. Gross, J. Raimond, C. Fabre, and S. Haroche, *Physical Review A* **27**, 2065 (1983).
- [16] A. Angerer, T. Astner, D. Wirtitsch, H. Sumiya, S. Onoda, J. Isoya, S. Putz, and J. Majer, *Applied Physics Letters* **109**, 033508 (2016).
- [17] J. R. Ball, Y. Yamashiro, H. Sumiya, S. Onoda, T. Ohshima, J. Isoya, D. Konstantinov, and Y. Kubo, *Applied Physics Letters* **112**, 204102 (2018).
- [18] W. Hardy and L. Whitehead, *Review of Scientific Instruments* **52**, 213 (1981).
- [19] B. Julsgaard and K. Mølmer, *Physical Review A* **86**, 063810 (2012).
- [20] K. Sandner, H. Ritsch, R. Amsüss, C. Koller, T. Nöbauer, S. Putz, J. Schmiedmayer, and J. Majer, *Physical Review A* **85**, 053806 (2012).
- [21] H. J. Carmichael, *Statistical methods in quantum optics 1: master equations and Fokker-Planck equations*, Vol. 1 (Springer Science & Business Media, 1999).
- [22] J. Choi, S. Choi, G. Kucsko, P. C. Maurer, B. J. Shields, H. Sumiya, S. Onoda, J. Isoya, E. Demler, F. Jelezko, N. Y. Yao, and M. D. Lukin, *Phys. Rev. Lett.* **118**, 093601 (2017).
- [23] T. Astner, J. Gugler, A. Angerer, S. Wald, S. Putz, N. J. Mauser, M. Trupke, H. Sumiya, S. Onoda, J. Isoya, *et al.*, *Nature materials* **17**, 313 (2018).
- [24] C. Gardiner and P. Zoller, *Quantum noise: a handbook of Markovian and non-Markovian quantum stochastic methods with applications to quantum optics* (Springer Science & Business Media, 2004).
- [25] L. Moi, P. Goy, M. Gross, J. Raimond, C. Fabre, and S. Haroche, *Physical Review A* **27**, 2043 (1983).
- [26] S. O. Rice, *The Bell System Technical Journal* **24**, 46 (1945).
- [27] E. A. Cooper and H. Farid, “A toolbox for the radial and angular marginalization of bivariate normal distributions, arxiv:2005.09696,” (2020).

Supplemental Material:

Triggered Superradiance and Spin Inversion Storage in a Hybrid Quantum System

SYSTEM HAMILTONIAN, EQUATIONS OF MOTION AND NUMERICAL MODELLING

Our system is described by the driven Tavis-Cummings Hamiltonian in the rotating frame [20],

$$\mathcal{H} = \hbar \Delta_c a^\dagger a + \frac{\hbar}{2} \sum_j \Delta_s^j \sigma_z^j + \hbar \sum_j g_0 (\sigma_-^j + \sigma_+^j a^\dagger) + i\hbar \eta (a^\dagger - a), \quad (\text{S1})$$

with a^\dagger (a) being the creation (annihilation) operator of the cavity mode and σ_z^j , σ_\pm^j being the Pauli- z and raising/lowering operators for the j^{th} spin, respectively. The spins are coupled to the cavity with constant coupling $g_0 = g_{\text{coll}}/\sqrt{N}$, where g_{coll} is the collective coupling strength and N is the number of spins. The spin detunings $\Delta_s^j = [\omega_s^j + \delta(t)] - \omega_p$ account for the inhomogeneous broadening of the spin ensemble and the additional shift $\delta(t)$ caused by the detuning loop, while $\Delta_c = \omega_c - \omega_p$ is the detuning of the cavity mode. Both detunings are calculated with respect to the driving frequency ω_p . Further, the amplitude of the driving field is determined by η . Using a Lindblad master equation, we take into account the loss rate κ for the cavity mode and the spin decoherence rate γ_\perp , thus yielding a set of coupled equations describing the dynamics of the operators,

$$\dot{a} = -(\text{i}\Delta_c + \kappa)a - \text{i} \sum_j g_0 \sigma_-^j + \eta, \quad (\text{S2})$$

$$\dot{\sigma}_-^j = -(\text{i}\Delta_s^j + \gamma_\perp) \sigma_-^j + \text{i} g_0 a \sigma_z^j, \quad (\text{S3})$$

$$\dot{\sigma}_z^j = 2\text{i} g_0 (\sigma_-^j a^\dagger - a \sigma_+^j). \quad (\text{S4})$$

Identifying these operators with their expectation values, effectively neglecting correlations between individual spins and the cavity by separating higher order moments into products of their first order counterparts, yields the well known Maxwell-Bloch equations. These equations of motion represent a semi-classical description of our system's dynamics, which can be solved numerically, e.g., to model the response to external stimuli. In our analysis, this description only fails to capture the stochastic nature of the inverted state's initial conditions.

To perform the numerical simulations, we approximate the spin frequency distribution $\rho(\omega)$, which is quasi-continuous due to the large number of spins, by sampling it at 1500 frequencies ω_j with equidistant spacing $\Delta\omega$. The resulting weights $\rho_j = \rho(\omega_j)\Delta\omega$ are then used to calculate the number of spins, $n_j = \rho_j N$, for each frequency bin ω_j . Assuming identical initial conditions for all spins

of one bin, also their dynamics according to Eqs. (S3) and (S4) are identical, thus tremendously reducing the number of relevant equations.

We determine the parameters describing our system, namely ω_c , κ , g_{coll} , and Γ_\perp [combining γ_\perp and the spin frequency distribution in one parameter, see Eq. (S5)] by fitting the steady state solution of the Maxwell-Bloch equations to the transmission signals [c.f. Fig. S4(a)], obtained with a vector network analyzer (VNA).

For modelling SR emission dynamics on short timescales, we can safely neglect T_1 processes, i.e., we do not include these in the master equation.

SPIN FREQUENCY DISTRIBUTION

We model the inhomogeneously broadened spin distribution $\rho(\omega)$ with a q-Gaussian function [20] with shape parameter $q = 1.39$ and FWHM of $\gamma_q/2\pi = 11$ MHz. The effective linewidth, present in the definition of the cooperativity $C = g_{\text{coll}}^2/\kappa\Gamma_\perp$ in the main text, can be calculated using [19]

$$\Gamma_\perp = \left[\int_{-\infty}^{+\infty} \frac{\rho(\omega) d\omega}{\gamma_\perp + \text{i}(\omega - \omega_0)} \right]^{-1}, \quad (\text{S5})$$

with ω_0 being the spin center frequency, together with the value for $\gamma_\perp/2\pi = 208$ kHz.

INITIALIZATION PROCEDURE AND INVERSION PULSE

All four NV sub-ensembles are tuned into resonance with the cavity using a vector magnet together with the detuning loop. As the third level of the NV ground state manifold is far away from resonance, we can treat the NVs as effective two-level systems. For all experiments, the spins are initialized close to their ground state by waiting 3 min after repeatedly sweeping a MW tone across the cavity resonance for 30 s, decreasing the cooperativity by roughly 25% but reducing wait times between different runs.

Starting from this state, the spins are inverted using an in-phase and quadrature modulated MW pulse. Similar to adiabatic fast passage methods for spins in free space, the starting point for the design of our inversion pulse is a chirped pulse of length 400 ns with a Gaussian envelope, that covers a frequency interval of about -8 to +8 widths γ_q . As our spins are not in free space but strongly coupled to a cavity, we cannot use the chirped pulse directly but need to adapt it for this circumstance. Comparing the

Maxwell-Bloch equations above with the optical Bloch equations, describing a two-level-system in free space driven by a classical coherent light field with driving amplitude $\Omega(t)$,

$$\dot{\sigma}_- = -\gamma_- \sigma_- + i\Omega(t)\sigma_z, \quad (\text{S6})$$

$$\dot{\sigma}_z = 2i(\Omega(t)\sigma_- - \Omega^*(t)\sigma_+), \quad (\text{S7})$$

we can see that the role of the driving amplitude in the case of the coupled cavity-spin system is taken by the term $g_0 a^\dagger$. Disregarding g_0 as a proportionality constant that has to be determined experimentally, we can assume a desired photonic amplitude $a(t) = a_R + ia_I$ given by the aforementioned chirped pulse and numerically solve for MW drive $\eta(t) = I - iQ$ necessary to create it in the cavity (see Fig. S1). Strictly speaking, this approach produces the correct effective inversion drive only for the spins with the center frequency, as only these are fully resonant. For other frequencies, the cavity acts as a filter and reduces the amplitude of the drive. Nevertheless, as the chirped pulse comes with a certain robustness to amplitude deviations, we still get a useful inversion efficiency for the whole spin ensemble. In the experiment, we scan the inversion pulse power to select the value for optimum inversion, which is in turn visible as the highest SR decay maximum for a given hold time.

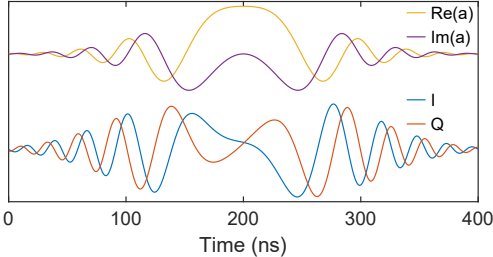


FIG. S1. Chirped pulse for initial spin inversion, desired $\langle a(t) \rangle$ and corresponding I/Q channels for optimal inversion.

DELAY TIME OF THE SUPERADIANT EMISSION

To derive Eq. (3) in the main text, we neglect the inhomogeneous broadening $\Delta_s^j \approx 0$ and describe the spin ensemble as a giant dipole using $S_\pm = \sum_j \sigma_\pm^j$ and $S_z = \frac{1}{2} \sum_j \sigma_z^j$. When inserting Eq. (S2) into Eq. (S4) on resonance $\Delta_c = 0$, we get

$$\dot{S}_z = -\frac{2g_0^2}{\kappa} S_+ S_- - \frac{ig_0}{\kappa} (S_+ \dot{a} - \dot{a}^\dagger S_-), \quad (\text{S8})$$

where we now can neglect the second term as it is of lower order in the number of spins $N \propto S_-$. Effectively, the cavity acts similar to a vacuum environment for the SR burst, although enhancing the coupling of individual spins

to the electromagnetic field. Its ability to store photons becomes of importance only at later times, when the cavity amplitude shows revivals, with excitations oscillating back and forth between cavity and spins. Then, we evaluate [13]

$$\begin{aligned} \langle \dot{S}_z \rangle &= -\frac{2g_0^2}{\kappa} \langle S_+ S_- \rangle \\ &= -\frac{2g_0^2}{\kappa} (S + \langle S_z \rangle) (S - \langle S_z \rangle + 1). \end{aligned} \quad (\text{S9})$$

By parametrizing $\langle S_z \rangle = \cos(\theta)N/2$ with a tipping angle θ and using $S = N/2$, we can now solve for the delay time t_D where $\langle S_z \rangle = 0$, as the SR emission reaches its maximum when the giant dipole points to the equator. The resulting expression [2, 15]

$$t_D = t_0 - \frac{\kappa}{2g_0^2 N} \log \left(\tan^2 \left(\frac{\theta}{2} \right) \right) \quad (\text{S10})$$

already resembles the one given in the main text. Now we linearize $\tan \theta \approx \theta$, neglect the constant offset t_0 and summarize the prefactor as $T_R = \frac{\kappa}{2g_0^2 N}$, representing the timescale of the SR emission process. We find good qualitative agreement of Eq. (S10) with our results. Quantitatively, when using the explicit values for κ and $g_0^2 N = g_{\text{coll}}^2$, the timescale of the SR emission is underestimated due to the approximations involved (in particular, neglecting the inhomogeneous broadening).

POST-SELECTION AND PHASE CORRECTION OF THE DECAY PULSES

The data collected in all experimental runs has some variance in the SR decay amplitudes. We assume this variance comes mostly from the solenoid switch located at the 1 K stage which is used to disconnect the the pump line from port 1 of the cavity after the inversion pulse. The switch opens and closes a mechanical connection by a latching mechanism, thus leading to slightly different initial ensemble inversions between the runs. The initial inversion S_z is what determines the length of the S_- component during the SR decay process, which in turn directly determines $\max(|a|)$ [see Eq. (S2)]. To account for these inversion imperfections, we post-select the data such that the maximum decay amplitudes fall in a narrow interval, as shown in Fig. S2(a).

The N appearing in Eq. (S10) can be taken to parametrize the initial inversion, and therefore also $\max(|a|)$. Solving Eq. (S10) for N , we therefore can deduce the functional relation between the maximum cavity amplitude and the delay time, $\max(|a|) = C/(t_0 - t_D)$, for a given tipping angle. We confirm this dependency by fitting the data of the highest power probe pulses in Fig. S2(a). The dependency of the delay time on the inversion clearly necessitates a post-selection, as not to

conflate this effect with the influence of the trigger pulse power in shifting the delay time t_D .

The linear shift of the SR decay phase with t_D [see Fig. S2(b)] comes from a slight detuning between cavity and spins and is corrected for in the data presented in the main text for clarity.

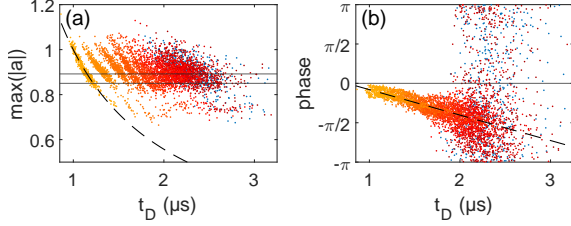


FIG. S2. (a) All recorded data points of the SR decay amplitude maxima $\max(|a|) = \sqrt{I_D^2 + Q_D^2}$ and phases $\varphi = \arctan(Q_D/I_D)$ over the delay time t_D , with the same color scheme as in the main text. The dashed line is a fit of the expected functional dependency to the highest power probe pulse values. The post-selected data points presented in the main text lie between the two horizontal lines. (b) Phase drift over delay time with a linear fit to the six highest probe pulse powers. This drift is corrected by a linear shift that aligns the dashed line with the horizontal axis.

DISTRIBUTION FUNCTIONS FOR DELAY TIME t_D AND PHASE ϕ OF THE SR DECAY

As described in the main text, the initial state of the inverted collective spin vector is located near the north pole of the Bloch sphere, close to the z -axis. Now, we approximate the surface near the north pole as a plane. Prior to the trigger pulse acting on the spin vector, the tipping angle $\theta = \arctan(|S_-|/S_z)$ is centered around $\theta = 0$ but with a finite width of $\bar{\theta}$. After the trigger pulse displaces the spin state, the tipping angle follows the Rician distribution [26]

$$f_\Theta(\theta, \eta, \bar{\theta}) = \frac{\theta}{\bar{\theta}^2} \exp\left(-\frac{1}{2} \left(\frac{\theta^2}{\bar{\theta}^2} + \eta^2\right)\right) I_0\left(\frac{\theta\eta}{\bar{\theta}}\right), \quad (\text{S11})$$

with the modified Bessel function of the first kind I_0 . The parameter η expresses the displacement of the initial spin vector away from the origin in units of the width parameter $\bar{\theta}$, which we assume to be in the direction $\phi = 0$. This displacement is a result of the spin rotation caused by the trigger pulse. For $\eta \gg 1$ the distribution f_Θ becomes a Gaussian with mean value $\langle \theta \rangle = \eta \bar{\theta}$ and variance $\text{Var}(\theta) = \bar{\theta}^2$. The angular distribution for $\phi = \arg(S_-)$ of the resulting in-plane vector is given by [27]

$$f_\Phi(\phi, \eta) = \frac{\eta}{\sqrt{2\pi}} \tilde{\varphi}(\eta) \left(1 + \eta \cos(\phi) \frac{\tilde{\Phi}(\eta \cos(\phi))}{\tilde{\varphi}(\eta \cos(\phi))} \right), \quad (\text{S12})$$

with the standard normal distribution $\tilde{\varphi}$ and its cumulative distribution function $\tilde{\Phi}$. As η increases, the initially randomly distributed angle ϕ becomes more and more well defined and approaches $\phi = 0$.

We can infer the initial tipping angles θ from the delay times t_D using a simplified expression for the delay time derived above

$$t_D = -2T_R \log\left(\frac{\theta}{2}\right), \quad (\text{S13})$$

depending only on θ and T_R . By applying a change of variables we arrive at the distribution for the delay times t_D

$$f_{t_D}(t_D, \eta, \bar{\theta}) = f_\Theta(\theta(t_D, T_R), \eta, \bar{\theta}) \left| \frac{d\theta(t_D, T_R)}{dt_D} \right|. \quad (\text{S14})$$

MICROWAVE SETUP

For the generation of our MW inversion pulses, we use an arbitrary waveform generator to modulate the I/Q -quadratures onto a carrier wave created by a power source generator (PSG) at the cavity frequency of 3.1 GHz. The pulses are gated using a fast MW switch, pass through a chain of digital attenuators and are amplified using a high power amplifier (+40 dB), before they enter the pump MW line, leading into the cryostat. At the 1 K stage inside the cryostat there is a relay switch, which can be used to completely decouple the pump line from the lower stages, blocking the room temperature thermal photons and the amplifier noise, which takes about 1 ms.

The probe pulses are created with another PSG and gated using a fast MW switch. Subsequently they pass through a second chain of variable digital attenuators, after which they are sent through the probe-line. In the experiment the probe-line has a fixed attenuation of -72.5 dB, of which -20 dB are located right outside the cryostat, the rest distributed among the stages. The probe-line is connected to cavity port 2 using a splitter, together with the out-line.

Following the out-line upwards, we have two MW isolators with a combined isolation of -20 dB and a -10 dB attenuator, for reducing thermal noise photons from the higher stages, before the signal is amplified with a low noise cryogenic amplifier. The signal is then demodulated using a homodyne detection setup, with the demodulation frequency supplied by the probe PSG. The two quadrature channels are finally measured with a high-speed data-acquisition system.

ESTIMATING THE NUMBER OF PHOTONS

To estimate the number of photons contained in a probe pulse we do a calibration measurement of the attenuation

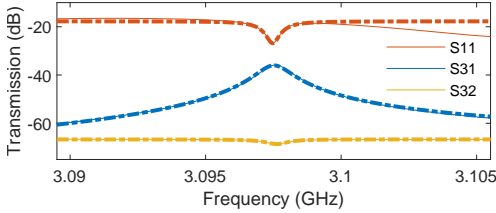


FIG. S3. S -parameter traces (solid lines) of the cavity with far detuned spins where the numbers 1, 2 and 3 correspond to the pump, probe, and out-line and their respective fits (dashed lines). For these measurements an additional -20 dB attenuator at the probe-port entry was removed. This does not change the values for $\kappa_{1,2}$ obtained by fitting the dips, as they appear only relative to the base level. The parameter κ_{tot} manifests itself in the HWHM of the Lorentzian peak of S_{31} .

$A_2 = -54.5$ dB + 2 dB at room-temperature for the probe-line inside the fridge up to port 2 of the cavity, where a value of +2 dB is added to account for the decreased resistance of the lines when cold. Then we determine the MW power for the strongest probe pulses of the signal that enters the probe-line outside the fridge using a power spectrum analyzer, $P_{\text{max}} = -58$ μW . The other probe pulses used in the experiment have variable attenuation decrements of -5 dB each, so the photon numbers change accordingly down to -45 dB relative to the highest power value.

Next, we determine the ratio R_2 of MW power reflected at cavity port 2 versus the incident power. For that, we measure the S -parameters of our system on resonance at 25 mK with the spins far detuned using the VNA as summarized in Fig. S3. By fitting the measured traces with the expected results from cavity input-output theory (reproduced for $\Delta_c = 0$, i.e., on resonance condition) [24] we obtain R_2 .

$$\begin{aligned} |S_{11}|^2 &= A_1^2 (2\kappa_1/\kappa_{\text{tot}} - 1)^2 \\ |S_{31}|^2 &= A_1 A_3 (2\sqrt{\kappa_1 \kappa_2}/\kappa_{\text{tot}})^2 \\ |S_{32}|^2 &= A_2 A_3 \underbrace{(2\kappa_2/\kappa_{\text{tot}} - 1)^2}_{= R_2} \end{aligned} \quad (\text{S15})$$

Here, the subscripts in $A_{1,2,3}$ refer to the fixed MW line attenuations inside the cryostat for pump, probe, and out-line respectively.

TABLE I. Summary of the parameters used to estimate the number of photons entering the cavity via the 100 ns trigger pulses through the probe-line.

$\kappa_2/2\pi$	$\kappa_{\text{tot}}/2\pi$	R_2	A_2	$P_{\text{max}}^{-45 \text{ dB}}$
59 kHz	586 kHz	0.64	-52.5 dB	1.83 nW

In a pulse with duration $\Delta t = 100$ ns, as used in the experiment, the number of photons that enter through

TABLE II. Parameters used to estimate the number of photons per pulse in the pulse sequences injected via the pump-line. As this experiment was done in another cool-down of our cryogenic system, the Q-factor of the resonator, therefore the κ_{tot} value, exhibits some deviations from the ones above.

$\kappa_1/2\pi$	$\kappa_{\text{tot}}/2\pi$	R_1	A_1	P_{MW}
182 kHz	516 kHz	0.086	-13.6 dB	2.1 μW

TABLE III. Temperatures of the various stages inside the dilution refrigerator and corresponding attenuations between the respective stages to estimate the number of thermal cavity photons, when the solenoid switch at the nominal 1 K stage is disconnected.

stage i	1	2	3	4	5	6
T_i (K)	296	42	4	0.9	0.12	0.025
$A_{i,i+1}$ (dB)						
pump	—	—	—	-2.5	-2	
probe	-2	-22	-2	-12	-14.5	
out	-2	-2	-2	-2	-30	

port 2 into the cavity using the lowest probe powers with -45 dB attenuation is then calculated as (c.f. Table I)

$$n_{\text{trig}}^{\text{min}} = \frac{P_{\text{max}}^{-45 \text{ dB}} \Delta t}{\hbar \omega_c} A_2 (1 - R_2) \approx 180.$$

For the pulse train measurements in the reduced cooperativity regime we use the same procedure to calculate the number of photons per 100 ns pulse entering through the pump-line (c.f. Table II),

$$n_{\text{trig}}^{pC < 1} = \frac{P_{\text{MW}} \Delta t}{\hbar \omega_c} A_1 (1 - R_1) \approx 4.1 \times 10^9.$$

Lastly, we calculate an estimate for the number of thermal photons in the cavity, when the solenoid switch at the 1 K stage is open to decouple the higher temperature stages. We use the values of Table III and evaluate according to

$$\begin{aligned} n_i &= \bar{n}(T_i) + A_{i-1,i} n_{i-1}, \\ \bar{n}(T) &= \frac{1}{\exp(\hbar \omega_c/k_B T) - 1}, \end{aligned} \quad (\text{S16})$$

going down the stages for all MW lines. The dominant contribution are thermal photons from the 1 K stage of the pump-line, which result in a value of $\bar{n} \approx 2.3$ photons.

T₁ MEASUREMENTS USING THE VECTOR NETWORK ANALYZER

In the main text we discuss a fast relaxation of the stored spin inversion with a characteristic timescale of 7.6 ms. This observed fast decay is contrasted by a slow relaxation from an approximately thermally mixed state,

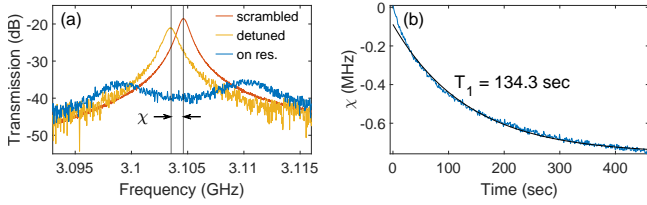


FIG. S4. (a) VNA transmission measurement of the hybrid system in its ground state on resonance (blue), with the detuning loop off (spins detuned, yellow) and measured using high input power to scramble the spins (red). (b) Dispersive shift χ over time, extracted from Lorentzian fits to the transmission data. The black fit line corresponds to a simple exponential decay law.

as shown in Fig. S4. The initial state for measuring this slow relaxation is created by repeatedly sweeping across the resonance with the VNA using a high input power for 30 s. This way, we scramble the spins, creating a state that resembles a thermal ensemble. For a large ensemble detuning $\delta \gg g_{\text{coll}}$ the dispersive shift χ , represented graphically in Fig. S4(a), allows a direct way to determine the long T_1 time of the spins with the result

$$\chi(t) = \frac{g_{\text{coll}}^2}{\delta} \langle S_z(t) \rangle, \quad (\text{S17})$$

as similarly employed in [23].

NITROGEN VACANCY CENTER SPINS AND DIAMOND SAMPLE

The spin ensemble used in this work consists of negatively charged nitrogen vacancy centers in diamond (NV), which are made up of a substitutional nitrogen atom with an adjacent lattice vacancy. This paramagnetic impurity has an electron spin $S = 1$ and can be described by the Hamiltonian $H = \hbar D S_z^2 + \mu B S$, with the zero field splitting $D = 2.88$ GHz and $\mu = 28$ MHz/mT. The diamond symmetry results in four possible orientations of the NV centers. In the present experiment the external magnetic field orientation was chosen to tune all four sub-ensembles into resonance with the cavity.

The roughly cube shaped diamond samples with side length $d \sim 200$ μm were cut from a larger sample by Delaware Diamond Knives. The larger sample was created similarly to the one characterized in detail in [23], referred to as “N1” therein. It was made by irradiating a commercially available high-pressure high-temperature diamond with an initial nitrogen concentration of 200 ppm and naturally abundant ^{13}C isotopes with our in-house neutron source (TRIGA Mark II reactor) for lattice vacancy creation. It was irradiated with a fluence of $5 \times 10^{17}\text{cm}^{-2}$ for 50 h and annealed at 900 °C for 3 h, resulting in a NV density of 40 ppm.